

# Investigation of the Kinetics of Pressure Coal Char Hydrogasification

Stanisław Gil <sup>1,\*</sup> , Wojciech Bialik <sup>1</sup>, Piotr Mocek <sup>1</sup>, Miroslav Rimár <sup>2</sup>, Ján Kizek <sup>2</sup>  and Nikolas Polivka <sup>2</sup> 

<sup>1</sup> Faculty of Engineering Materials, Silesian University of Technology, Krasińskiego 8, 40-019 Katowice, Poland; wojciech.bialik@polsl.pl (W.B.); piotr.mocek@polsl.pl (P.M.)

<sup>2</sup> Department of Process Technique, Faculty of Manufacturing Technologies with a Seat in Presov, Technical University of Kosice, Bayerova 1, 080 01 Presov, Slovakia; miroslav.rimar@tuke.sk (M.R.); jan.kizek@tuke.sk (J.K.); nikolas.polivka@tuke.sk (N.P.)

\* Correspondence: stanislaw.gil@polsl.pl; Tel.: +48-32-603-4221

**Abstract:** The authors of the study focused on the problem of hydrogasifying coal extracted from a particular location. Since hydrogen is transparent to radiation, it can only be heated by convection. To achieve this, we developed a swirler and utilized Fluent software (version 19.0) to simulate the primary flow vectors and the temperature distribution of hydrogen in the hydrogasification reactor. The process was carried out under varying conditions, including temperatures ranging up to 1173 K, pressures of up to 8 MPa, and gas flow rates between 0.5 and 5 dm<sup>3</sup> min<sup>-1</sup>. The results showed that the carbon reactivity of the char was high up to a certain level of carbon conversion. In this study, the kinetic equations of the hydrogasification process were developed based on the theory of active centers. The researchers also evaluated the kinetic constants at the maximum reaction rate for the analyzed chars. The analysis was conducted for four extreme cases of process parameters, which included temperatures of 973 and 1173 K as well as pressures of 6 and 8 MPa. The results showed that the maximum hydrogasification reactivity of chars could be accurately described using equations for both the first- and second-order reactions toward hydrogen. This was likely due to the use of a narrow pressure range of 6–8 MPa during the experiments. The kinetic equations developed in the study could be used to model the process on a technical scale.

**Keywords:** hydrogasification; coal; char; kinetics



**Citation:** Gil, S.; Bialik, W.; Mocek, P.; Rimár, M.; Kizek, J.; Polivka, N. Investigation of the Kinetics of Pressure Coal Char Hydrogasification. *Energies* **2023**, *16*, 4937. <https://doi.org/10.3390/en16134937>

Academic Editor: Reza Rezaee

Received: 5 April 2023

Revised: 27 May 2023

Accepted: 21 June 2023

Published: 25 June 2023



**Copyright:** © 2023 by the authors. Licensee MDPI, Basel, Switzerland. This article is an open access article distributed under the terms and conditions of the Creative Commons Attribution (CC BY) license (<https://creativecommons.org/licenses/by/4.0/>).

## 1. Introduction

According to the Energy Union strategy (2015), one of the goals of the EU's energy policy is to focus on improving energy efficiency, reducing dependence on energy imports, and primarily reducing CO<sub>2</sub> emissions. In accordance with the Paris Agreement, another goal is to decarbonize the economy and transition to a low-carbon economy. However, these goals cannot be achieved without supporting research in the field of low-carbon and clean energy technologies. At the same time, research and innovation should be prioritized to stimulate energy transformation [1].

The current energy situation necessitates considering the utilization of all available energy sources. As part of the decarbonization and low-carbon technology strategy, EU countries have committed to phasing out the use of solid and liquid fossil fuels and replacing them with low-carbon fuels. Recently, attention has been focused on the production and utilization of hydrogen in various technologies as a means of reducing CO<sub>2</sub> emissions.

Returning to the idea of transforming solid and liquid fuels into low-carbon gaseous fuels is one alternative for promoting energy independence while simultaneously supporting more environmentally friendly technologies through further research into existing technologies. One of the discussed technologies is the gasification of solid fuels such as coal, biomass, and organic waste from municipal and industrial sectors. Tosti et al. [2] discussed the idea of producing alternative gaseous fuels as a substitute for natural gas using coal hydrogasification technology. In this publication, they correctly pointed out

the issue of the availability of hydrogen produced from renewable sources. Nevertheless, hydrogasification of coal can be considered one of the ways to reduce the import of natural gas into the EU.

Gasification of coal directly in underground deposits is an innovative idea that enables the use of fossil fuel resources that are not economically feasible to extract using traditional methods. Researchers [3] have extensively studied this area, developing a physical model to investigate various factors that affect the gasification process. In their work [4], the authors explore the use of hydrogasification in underground deposits by conducting experiments that simulate the conditions of underground gasification. However, research in the field of underground gasification has highlighted the formation of tar as the primary challenge in obtaining clean synthesis gas. Nevertheless, research results indicate possible solutions to mitigate tar formation. Wiatowski [5] conducted experimental studies on the underground coal gasification (UCG) process to analyze the formation of tar quantitatively and qualitatively. Tar formation is a notable issue in biomass gasification. The findings of a previous study by the authors [6] indicated that this is primarily a concern with countercurrent gasifiers and that the solution lies in transitioning to a co-flow gasifier to mitigate tar formation.

Mlonka-Medrała et al. [7] focused on improving the quality of synthesis gas from agricultural waste biomass; the results of experimental measurements and numerical simulations confirmed the influence of temperature on the purity of synthesis gas in this case as well. In his work, Slovak [8] emphasized that modern methods of theoretical description of the process will not allow the prediction of good results if they are not based on experimental data that take into account the specific conditions of the gasification process. By comparing the methods of mathematical modeling, he divided gasification processes into five types. These include methods based on the principle of basic kinetic laws, methods of thermodynamic equilibrium, thermodynamics, empirical simulation methods, and combined models.

Saraceno et al. [9] conducted a comprehensive review of various coal and biomass gasification methods, with a particular emphasis on hydrogasification. The review focused on examining the impact of different factors, including catalytic gasification, on the intensity of the hydrogasification process. Catalytic gasification has been extensively studied in several publications to determine the effects of catalysts on hydrogasification [10]. The primary objective of this research was to identify the optimal catalyst for achieving a high methane yield.

The hydrogasification process shows the possibility of generating natural gas substitutes from coal and is therefore a topic for deep investigation [11–15]. Two stages are involved in the hydrogasification of coal: in the first, coal pyrolysis occurs at an extremely fast rate under high pressure in an atmosphere of hydrogen, and the second is a comparatively slow phase with the hydrogasification of the char that is still present. In an inactive atmosphere, more quantities of liquid and gaseous hydrocarbons are obtained by hydrolysis than by pyrolysis [12,13,16].

Reactive activities of coal chars with hydrogen have undergone extensive research [17–22] in an effort to determine char features and gasification conditions that affect the rate of the reaction.

The outcomes of Tomita et al.'s [21] thermogravimetric analysis (TGA) hydrogasification studies on several chars showed that the more carbon conversion takes place, the more reactive most of the chars become, until the process attains a constant value at about 30% to 50% conversion; however, if there is only one char, the reactivity will decrease as carbon conversion proceeds. Nevertheless, Mühlen [20] and Mühlen et al. [23] observed that this decrease in reactivity as carbon conversion proceeds is specific to char hydrogasification. A previous study by Johnson [24] validated this assertion. Johnson discovered that the rate of hydrogasification is at its maximum shortly after coal devolatilization and declines as gasification increases.

According to Tomajian et al. [25], the hydrogasification rate rapidly declines as coal and other char are converted. Additionally, Gonzales et al. [15] observed a sharp decline in the hydrogasification rate, with a conversion of only about 40% at temperatures higher than 1023 K.

Hydrogen plays a crucial role in the first stage of coal gasification (hydropyrolysis) because of its impact on primary tar and the solid carbon skeleton. Even at comparatively low pressures, coal pyrolysis with hydrogen significantly enhances carbon conversion to gaseous hydrocarbons [26,27].

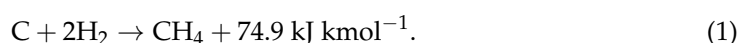
Studies have shown that catalyst-related advantages are specifically significant for these types of gasification processes, where the potency of the reaction cannot be increased by the traditional method of increasing temperature, such as direct coal gasification into methane or allothermal gasification using an external, diaphragm heat source [10,28–30].

The purpose of this research is to investigate the hydrogasification reactivity of chars formed from Polish subbituminous coal, which is promising for gasification to produce methane due to its significant deposits in southern Poland. The dynamics of the procedure were investigated to determine the kinetic constants at the maximal rate of formation of methane by the heterogeneous reaction of solid carbon with hydrogen. In light of this research, we suggest a model for the hydrogasification rate's speed that accounts for the variations in the porosity of the char and its inner surface, as well as its active centers. The experimental study focuses solely on the ongoing process and kinetics of hydrogasification. To achieve a more comprehensive understanding of the underlying processes, a CFD model was developed. The objective of the CFD model is to present the internal processes through temperature distribution and a vector representation of gas flow under specific operating temperature and pressure conditions. This highlights the significance of the reactor's internal construction, which also influences the hydrogasification processes.

## 2. Materials and Methods

### 2.1. Hydrogasification

The term “hydrogasification” refers to the exothermal reaction between hydrogen and carbon to form methane.



According to the laws of thermodynamic equilibrium in the  $\text{H}_2\text{-CH}_4\text{-C}$  system, the hydrogasification process must be carried out at high pressure  $p$  in order to produce a high molar proportion of methane  $z_{\text{CH}_4}$  in the  $\text{H}_2\text{-CH}_4$  solution, which results from the equilibrium constant  $K(T)$  of reaction (1):

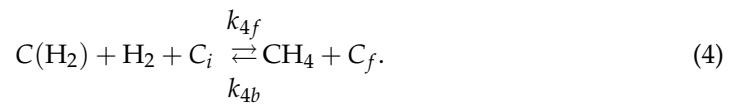
$$K(T) = \frac{z_{\text{CH}_4}}{z_{\text{H}_2}^2 \left(\frac{p}{p_n}\right)}, \quad (2)$$

where  $z_{\text{H}_2}$  is the molar proportion of hydrogen and  $p_n$  is the normal pressure (101,325 Pa).

Introduction of coal into a hydrogen-rich atmosphere with elevated temperature and pressure produces a two-stage process: a—hydropyrolysis, whereby volatile matter liberated from coal combines with hydrogen to form primary methane-rich gas and solid char, which is highly reactive during the early phase; b—hydrogasification of the char, with high initial reactivity that declines as gasification intensity increases.

The theory of active centers  $C_f$  is employed in the kinetic mechanism of hydrogasification, where the reactants and inactive centers  $C_i$  can be adsorbed. Blackwood [26] proposed a two-step mechanism:





In addition, he assumed that methane desorption in the reaction (4) determines the process rate. In his later paper [18], he changed this assumption to exclude the superiority of either. If  $[C_f]$  is the surface concentration of free active centers per 1 g of carbon and  $[C(H_2)]$  is the concentration of  $C(H_2)$ -coated active centers per 1 g of carbon, the rate of solid methane production ( $\dot{R}_i$  or  $\dot{R}$ ) in a steady state for a sample with the mass  $m_c$  can be determined as follows:

$$\dot{R}_3 = n_C \{k_{3f}[C_f]p_{H_2} - k_{3b}[C(H_2)]\}, \quad (5)$$

$$\dot{R}_4 = n_C \{k_{4f}[C(H_2)]p_{H_2} - k_{4b}[C_f]p_{CH_4}\}, \quad (6)$$

where  $n_C$  is the number of carbon moles, kmol;  $p_{H_2}$  is the partial pressure of hydrogen, Pa.

The solution of the system of Equations (5) and (6) can be presented in the following way:

$$\dot{R} = n_C \frac{\frac{k_{3f}k_{4f}}{k_{3b}}p_{H_2}^2 - k_{4b}p_{CH_4}}{1 + \frac{k_{3f}+k_{4f}}{k_{3b}}p_{H_2} + \frac{k_{4b}}{k_{3b}}p_{CH_4}}, \quad (7)$$

where  $p_{CH_4}$  is the partial pressure of methane, Pa.

For very small methane concentrations in the gasifying environment, the impact of  $CH_4$  on the hydrogasification rate can be neglected, and Equation (8) is simplified to the Langmuir-Hinshelwood equation:

$$\dot{R} = n_C \frac{Ap_{H_2}^2}{1 + Bp_{H_2}} \quad (8)$$

The hydrogasification rate for char attains its maximum value shortly after coal devolatilization and declines with gasification degree in accordance with the exponential function established by Johnson [24] that was modified by Mühlen [20] to the relationship between char gasification degree  $x$  and process temperature  $T$ -dependent:

$$\frac{\dot{R}(x)}{\dot{R}(x=0)} = \exp\left(-\frac{bx^2}{RT}\right) \quad (9)$$

where  $b = 17.5 \text{ kJ mol}^{-1}$ . Based on hydrogasification experiments on the char produced from subbituminous coal Fürst Leopold at 800 °C, conducted at 1 to 6 MPa and 800 to 1000 °C, Mühlen [4] determined the following values for Equation (8) defining the gasification rate:

$$A = 6.91 \cdot \exp\left(-\frac{a}{TR}\right), \left(\text{min} \cdot \text{MPa}^2\right)^{-1}; \quad (10)$$

where  $a = 72.1 \text{ kJ mol}^{-1}$ ,

$$B = 3.5 \cdot 10^{-6} \exp\left(-\frac{b}{TR}\right), \text{MPa}^{-1}; \quad (11)$$

where  $b = 118.1 \text{ kJ mol}^{-1}$ .

Pressure has a distinct effect on the rate of hydrogasification than it does during the gasification of  $H_2O$  and  $CO_2$ . According to calculations made under isothermal settings,  $t = 900 \text{ °C}$  as a function of pressure and as a function of temperature at the pressure  $p = 2 \text{ MPa}$ , Mühlen [20] compared the rates of the above three types of char gasification.

At only about 2 MPa, a typical maximal rate of char gasification in H<sub>2</sub>O and CO<sub>2</sub> was recorded. The H<sub>2</sub>O gasification rate is more than three times higher than the CO<sub>2</sub> gasification rate across the entire pressure range. Hydrogasification is the least rapid process at low pressures; it takes around 40 bar to accomplish the gasification rate in CO<sub>2</sub>, while approximately 10 MPa is needed to achieve the gasification rate in H<sub>2</sub>O.

Since there are significant quantities of Polish subbituminous coal in southern Poland, the gasification of this coal for the generation of methane is promising. The goal of the current study was to investigate the hydrogasification reactivity of chars formed from this coal. The primary objective of the study was to determine how the char conversion affected the reactivity of chars at varied temperatures and pressures. To determine the kinetic constants at the maximal rate of production of methane via the heterogeneous interaction of solid carbon with hydrogen, the kinetics of the process are investigated.

## 2.2. Experimental Facility and Heating Problems

Figure 1 shows an illustration of the experimental facility. A flow rate of 0.1 to 10 dm<sup>3</sup> min<sup>-1</sup> (normal cubic decimeter per minute) of pure hydrogen (or hydrogen mixed with another gas) is utilized in the pressure reactor (11) to hydrogasify samples up to 30 g. 1 K s<sup>-1</sup> electrical sample heating device installed in the reactor makes sure that hydrogen is heated to the process temperature simultaneously (up to 1273 K). The reactor is sterilized with helium and then filled with hydrogen after the sample has been inserted inside.

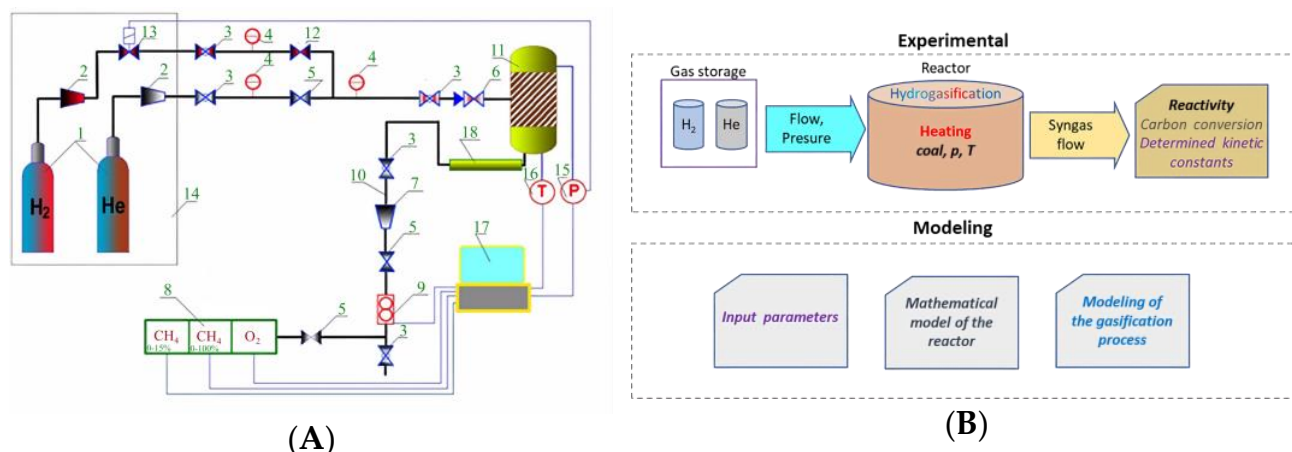


**Figure 1.** (A) Experimental facility: 1—gas cylinders, 2—pressure controller 30/10 MPa, 3—cut-off valve, 4—manometer, 5—control valve, 6—check valve, 7—pressure controller 25/1 MPa, 8—analyzer, 9—flow controller, 10—pipe, 11—reactor, 12—single-stage pressure controller, 13—electromagnetic valve, 14—gas cylinder cabinet, 15—pressure converter, 16—thermocouple, 17—computer, and 18—cooler. (B) Methodology flowchart.

The mass flow controller maintains the hydrogen flow rate at  $\pm 1.5\%$  (9). The analyzer calculates the amount of CH<sub>4</sub> in the process gas (8). The process variables are captured at predetermined intervals of 5 s. In Figure 2, the experimental facility is presented. The facility's module design makes sure that the measurement and flow channels for the process gases can be expanded further. It specifically makes sure that hydrogen solution and an additional reactant are supplied to the process.



**Figure 2.** A perspective of the experimental facility.

Chars were produced in a separate station intended for coal devolatilization. The station enables devolatilization of samples up to 1.5 g at a heating rate of  $1\text{--}100\text{ K s}^{-1}$  up to 1373 K and at up to 3 MPa in inert gas.

A serious problem with reactor operation was the inability to measure the actual temperature of hydrogen during hydrogasification, as  $\text{H}_2$  is transparent to radiation and only heats up through convection. There was a concern that the hydrogen temperature would be lower than the char temperature. It is necessary to expand the gas-reactor wall contact surface and the gas path in addition to directing the hydrogen flow. A swirler was designed for this purpose, and the mainstream vectors and hydrogen temperature fields in the hydrogasification reactor were modeled in Fluent, a program that enables the determination of spatial or surface flow parameters, physical quantity distributions defined in conservation equations, closing hypotheses, and equations of state. The numerical divisions applied in the program procedures are based on the finite volume method. It was developed based on universal algebraic equations obtained from differential equations for elementary surface or volume dimensions and (in the case of transient state calculations) the elementary time step. In Figure 3, the reactor design and its spatial arrangement are presented. The gas was delivered from the swirler. The reactor components were mostly heated up through radiative heat transfer. The mesh was divided into three zones: the inlet zone with the swirler, the char zone, and the outflow zone with the char-holding grate, which allow for modeling a fixed, deposited char bed. The marginal conditions and the mesh parameters are presented in Table 1.

Calculations were performed for two extreme cases, i.e.,  $700\text{ }^\circ\text{C}$  at 6 MPa and  $1000\text{ }^\circ\text{C}$  at 10 MPa. The dispersion of the thermal fields and flows in the reactor that was empty and the reactor that had 10 g of coal were taken into consideration for each scenario. Multiphase flow calculations were required during the modeling of the char-filled reactor, and the fixed bed having an average solid phase consisting of 0.8 mm particles (on average) was estimated. The other parameters for the char-containing reactor and the data on the char used in the modeling process are presented in Table 2.

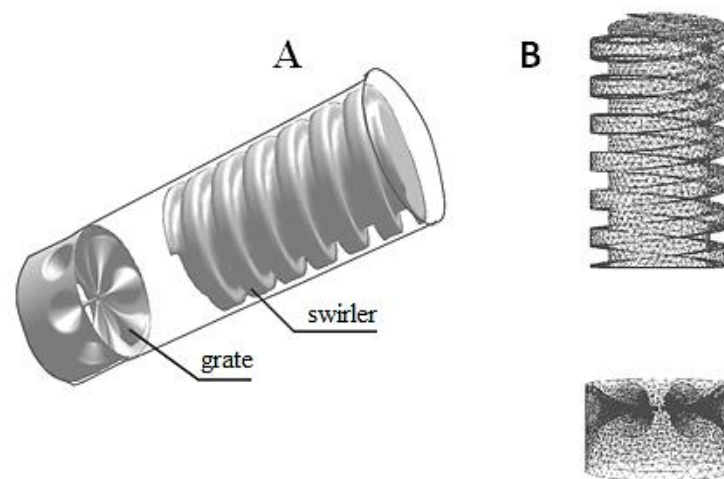


**Figure 3.** The design of reactor components (A), the numerical mesh on the surfaces of the swirler, and the outlet area (B).

**Table 1.** Main data of the model and characteristics of the discrete mesh.

Parameter, Unit	Value
Temperature of the swirler surface, min/max, °C	700/1000
Temperature of the quartz pipe wall, min/max, °C	700/1000
Number of the mesh elementary volumes	189,992
Volume of the largest elementary cell, m <sup>3</sup>	$9.364 \times 10^{-9}$
Volume of the smallest elementary cell, m <sup>3</sup>	$4.777 \times 10^{-16}$
Operating pressure, min/max, MPa	6/10
H <sub>2</sub> temperature at the reactor inlet, °C	19
Coefficient of convective transfer into the reactor/swirler walls, Wm <sup>-2</sup> K <sup>-1</sup>	132/145
Mass flow rate (the reactor), kg <sub>n</sub> h <sup>-1</sup>	26.4

**Table 2.** Main data for the modeling of biphasic gas flow through the char layer.

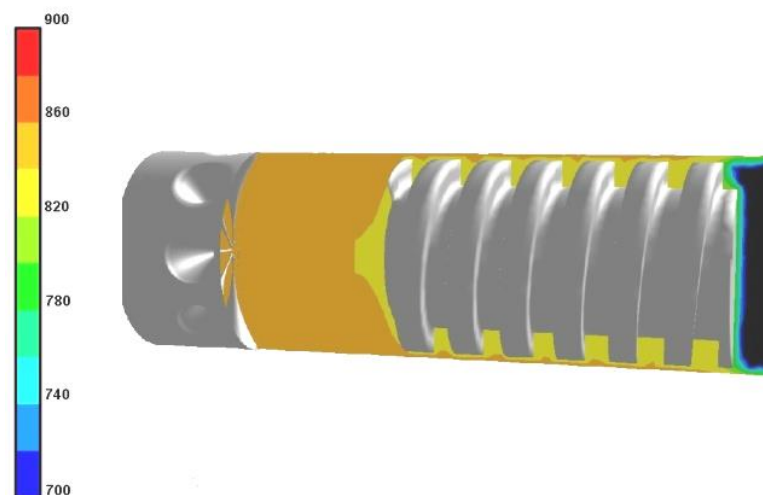
Parameter, Unit	Value
Number of phases	2
Mean porosity within the char bed	0.6
Emissivity of the char surface	0.95
Char mass, g	10
Initial temperature of the char surface, min/max, °C	700/1000
Turbulence model	Each of the phases k-ε
Char density, kg m <sup>-3</sup>	1400
Coefficient of convective transfer from hydrogen into the char, Wm <sup>-1</sup> K <sup>-1</sup>	132/145

Table 3 presents information about the computational methodology of CFD, such as pressure velocity coupling, discretization, relaxation factors, and mesh shape and structure. The increase in the number of discrete mesh elements was conducted until no further change in the calculation results occurred. It was assumed that subsequent calculation results should not differ by more than 1%. The condition  $EAS < 75\%$  was met for each of the tested meshes.

**Table 3.** Information about the computational methodology of CFD.

Parameter	Value
Pressure velocity coupling	Simple
Discretization	
Pressure	Presto
Momentum	Second order upwind
Volume fraction	Second order upwind
Turbulence kinetic energy	Second order upwind
Turbulence dissipation rate	Second order upwind
Energy	Second order upwind
Discrete ordinates	
Under relaxation factors	
Pressure	0.3
Density	0.4
Body forces	0.2
Momentum	0.4
Slip velocity	0.2
Vol. fraction	0.2
Turbulence kinetic energy, k	0.4
Turbulence dissipation rate, e	0.4
Turbulent viscosity	0.4
Energy	0.4
Discrete Ordinates	0.5
Mesh shape and structure	Tetrahedral, unstructured
Maximum equi-angle-skew factor (EAS) value of mesh	
Mesh shape and structure	0.80

The computations produced flow parameter fields specific to reactors operating under two extreme experimental scenarios (Figures 4–7).



**Figure 4.** The temperature field (in Kelvin degrees) in the hydrogasification reactor, with an operating temperature  $T = 973$  K and an operating pressure  $p = 6$  MPa.

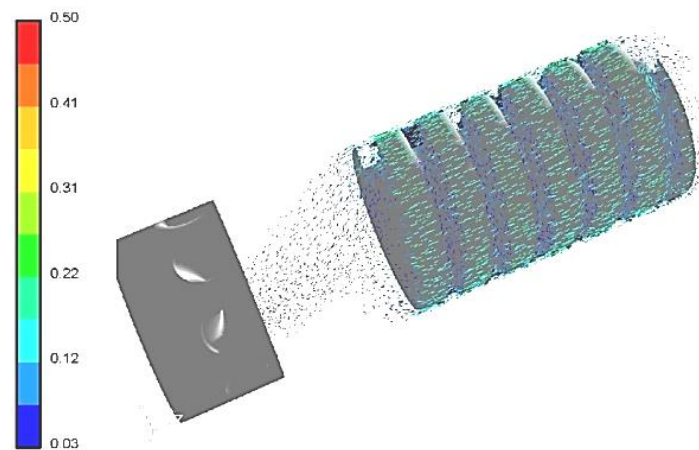


**Figure 5.** Vectors of the velocity ( $\text{m s}^{-1}$ ) of the gas stream in the hydrogasification reactor, with an operating temperature  $T = 973 \text{ K}$  and an operating pressure  $p = 6 \text{ MPa}$ .

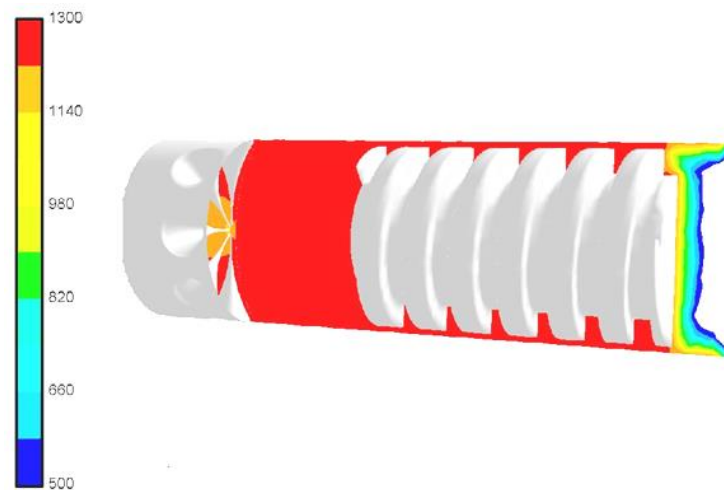


**Figure 6.** The temperature field (in Kelvin degrees) in the hydrogasification reactor, with an operating temperature  $T = 1273 \text{ K}$  and an operating pressure  $p = 10 \text{ MPa}$ .

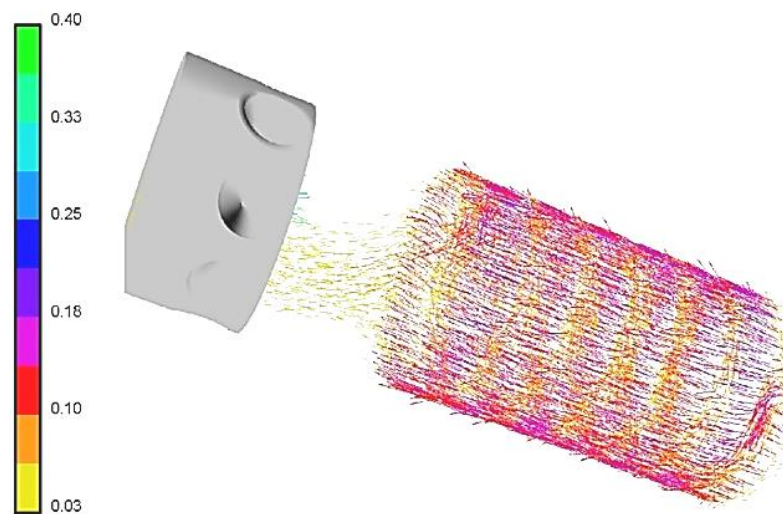


**Figure 7.** Vectors of the velocity ( $\text{m s}^{-1}$ ) of the gas stream in the hydrogasification reactor, with an operating temperature  $T = 1273 \text{ K}$  and an operating pressure  $p = 10 \text{ MPa}$ .

### 3. Experimental

The char was formed within 30 min of pyrolysis in helium at 2 MPa and 1373 K (heating rate: 100 K s<sup>-1</sup>). The char samples were separated into a category of 0.6–1.0 mm-sized particles by sieving. Janina, a subbituminous coal obtained from Silesia, was used for the experiments; see Table 4.

**Table 4.** Characteristics of the Janina coal [31].

W <sup>a</sup> , %	V <sup>a</sup> , %	A <sup>a</sup> , %	C <sup>a</sup> , %	H <sup>a</sup> , %	S <sup>a</sup> , %	N <sup>a</sup> , %
10.21	32.41	9.46	62.73	3.94	1.45	0.84

W<sup>a</sup> is water, V<sup>a</sup> is volatile matter, A<sup>a</sup> is ash, C<sup>a</sup> is carbon, H<sup>a</sup> is hydrogen, S<sup>a</sup> is sulfur, and N<sup>a</sup> is nitrogen, respectively, in the analytical state.

The initial properties of the Janina char (i.e., solid particle porosity,  $\epsilon_0$ ; internal specific surface area,  $A_0$ ; real density,  $\rho_0$ ; initial total active centers,  $C_{f0}$ ; carbon content in the analytical state,  $C^a_0$ ) used for testing the mechanism and the kinetic constants are presented in Table 5.

**Table 5.** Characteristics of the Janina char [32].

$\epsilon_0$	$A_0$	$\rho_0$	$C_{f0}$	$C^a_0$
%	m <sup>2</sup> kg <sup>-1</sup>	kg m <sup>-3</sup>	kmol <sub>a.c.</sub> kg <sup>-1</sup>	%
59.3	$16.7 \times 10^3$	1390	$16.1 \times 10^{-5}$	80.1

The experiments were conducted in accordance with the Janina coal hydrogasification schedule of 10 g of samples being subjected to 973 and 1073 K at a pressure of 8 MPa and at a hydrogen flow rate of 0.5 dm<sub>n</sub><sup>3</sup> min<sup>-1</sup>.

'Janina' coal samples weighing 10 g were used in the char hydrogasification assessments. The hydrogasification schedule involved trials for pressures of 6, 7, and 8 MPa with hydrogen flow rates of 0.5, 2, and 5 dm<sub>n</sub><sup>3</sup> min<sup>-1</sup> at 973, 1073, and 1173 K.

The rate of the hydrogasification reaction was determined using the measured molar methane (CH<sub>4</sub>) content. Given that H<sub>2</sub> was delivered into the reactor and that both H<sub>2</sub> and CH<sub>4</sub> are present in the observed molar gas stream  $\dot{n}_g$  leaving the reactor, the rate of hydrogasification—which is equal to the rate of CH<sub>4</sub> production—was estimated as follows:

$$\dot{R} = \dot{n}_g z_{CH_4} \quad (12)$$

The quantity of carbon moles present in the reactor's solid char at time  $t$  equals:

$$n_C(t) = n_C(0) - n_{CH_4}(t) \quad \text{kmol} \quad (13)$$

where  $n_C(0)$  is the initial quantity of carbon moles in the sample of char, and  $n_{CH_4}(t)$  is the quantity of moles of generated methane at time  $t$ .

Carbon conversion  $U(t)$  is defined as follows:

$$U(t) = 1 - \frac{n_C(t)}{n_C(0)} \quad (14)$$

Considering the degree of carbon conversion, the particle porosity  $\epsilon(t)$ , internal specific surface area  $A(t)$ , and total active centers  $U(t)$  can be determined. Based on Stanmore [33], it was assumed that:

$$\epsilon(t) = \epsilon_0 + U(t)(1 - \epsilon_0) \quad (15)$$

and

$$A(t) = A_0[1 + 2.5U(t)][1 - U(t)] \quad (16)$$

In the paper by Gil et al. [32], other relationships were proposed and verified based on the experimental data reported in [34]:

$$\varepsilon(t) = \varepsilon_0 \exp[-U(t) \ln(\varepsilon_0)] \quad (17)$$

$$A(t) = A_0 \exp \left\{ \begin{array}{l} -2U(t) \ln(\varepsilon_0) + \\ + a[1 - \exp(-U(t) \ln(\varepsilon_0))] \end{array} \right\} \quad (18)$$

$$C_f(t) = C_{f0} \frac{[1 - \exp(-U(t) \ln(\varepsilon_0))]}{1 - \varepsilon_0} \cdot \exp\{-2U(t) \ln(\varepsilon_0) + a[1 - \exp(-U(t) \ln(\varepsilon_0))]\} \quad (19)$$

where  $a$  is the matching constant for coals,  $a = 1 \pm 0.05$ . For active carbons, coals, and coal chars with high microporosity and anthracites, the suggested matching constant values are lower by approximately 40%.

Figure 8 shows how the hydrogasification isothermal stage temperatures (973, 1073, and 1173 K) at 6 MPa affect the rate of conversion of char for the Janina char.

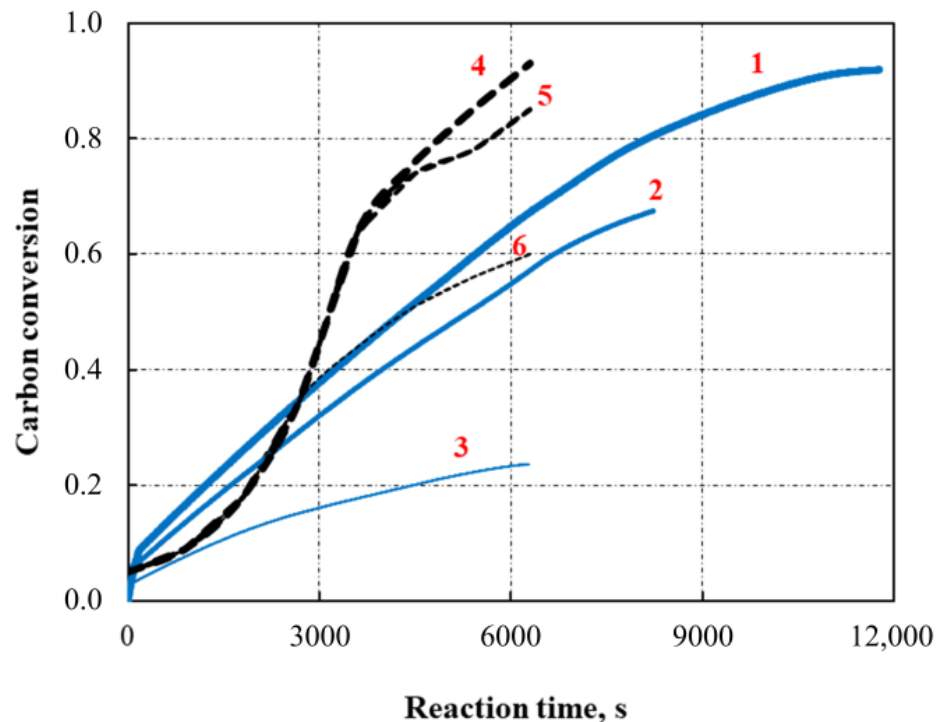


**Figure 8.** The influence of temperature on the carbon conversion rate in our own experiments, Janina char, 6 MPa: (1) 1173 K, (2) 1073 K, (3) 973 K; and Ding et al. [35], ‘Inner Mongolia Semicoke’, 5 MPa: (4) 1173 K, (5) 1073 K, (6) 973 K.

The results were contrasted with those reported by Ding et al. [35] for the ‘Inner Mongolia Semicoke’ under the same conditions and at 5 MPa. The highest conversion rate for the Janina char was similar to that reported by Ding et al., while it was lower by 18% at 1173 K.

Figure 9 shows the measured  $\text{CH}_4$  molar concentration at the reactor outflow for three different hydrogasification temperatures: 973, 1073, and 1173 K, as well as two different reaction pressure values: 7 and 8 MPa.

All three of the cases were equal in terms of the original char sample mass. The amount of methane in the resultant gas exiting the reactor is higher because a greater reaction pressure increases the production of methane.

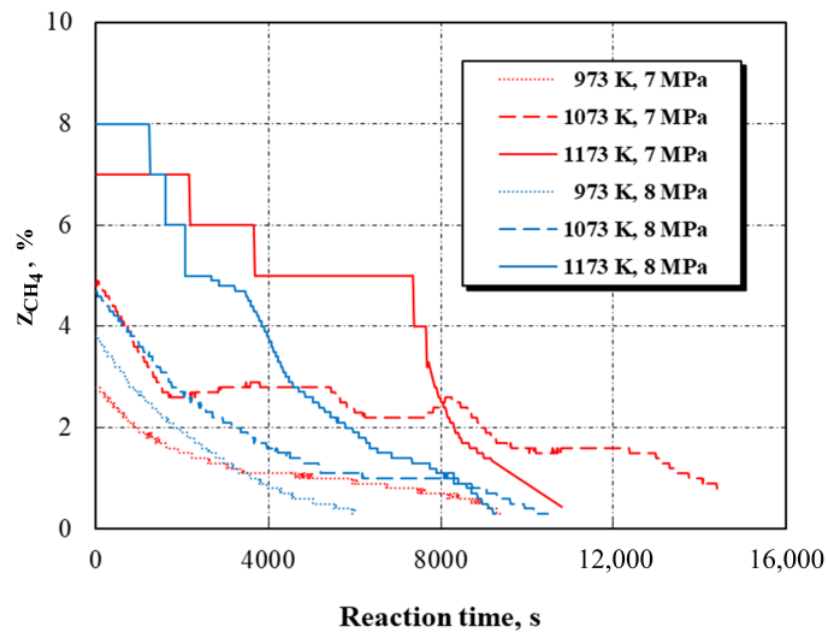


**Figure 9.** Molar methane content in the outflow gas measured as a function of time for the Janina char,  $2 \text{ dm}_n^3 \text{ min}^{-1}$ , 0.6–1.0 mm.

Figure 10 shows the computed char reactivity for two temperature values, 1073 K and 1173 K, which is defined as the ratio  $\dot{R}/n_c(t)$ , and the hydrogasification pressure of 7 MPa and 8 MPa as a function of carbon conversion determined by the ratio  $U(t)$ . When the C conversion exceeds 60% or 80%, respectively, for 1073 K and especially for 1173 K, the reactivity rapidly decreases. This implies that a temperature of roughly 1200 K needs to be maintained in order to achieve a significant amount of C conversion during char hydrogasification.

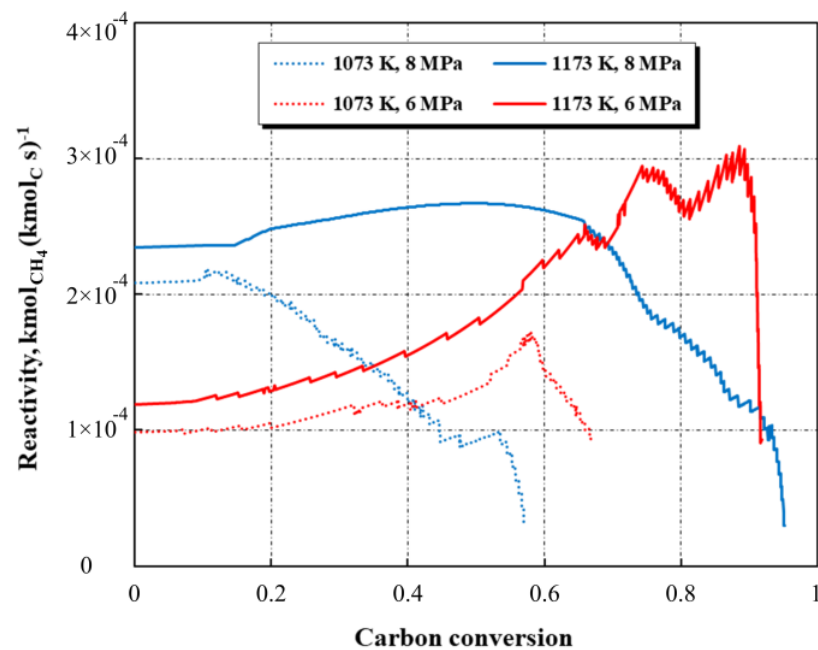
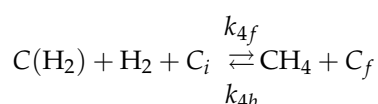
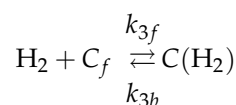


**Figure 10.** Hydrogasification reactivity versus carbon conversion: the Janina char,  $2 \text{ dm}_n^3 \text{ min}^{-1}$ , 0.6–1.0 mm.

#### 4. Kinetics of Char Hydrogasification

For chars, the role of the active center may be attributed to the marginal carbon atoms in the coal structure, dislocations, infinite inclusions, or oxygen or hydrogen groups.

The development of the kinetic relationships in the char particle-gas reaction requires the analysis of elementary phenomena on the solid-gas surface, which is possible based on the theory of active centers. Porous char particles react with gas on the external surface and inside the pore structure. Active centers formed by irregularities in the particle surface trigger gas-solid bonding or adsorption. Reactant adsorption, intermediate migration, and product desorption may occur in any active center. As a result of the reactant  $X$  adsorption, the free active centers become the occupied centers  $C(X)$ . In his later paper on the hydrogasification process within the range of 923 K to 1143 K, Blackwood [17] discusses the mechanism, which is expanded by two further reactions:



when this mechanism is simplified and only involves reactions (3) and (4), simple relationships determining the gasification rate expressed in moles of solid carbon proceeding to the solid phase as methane can be obtained. The presence of the reactions (20) and (21) is justified by the fact that the reaction between the carbonate and atomic hydrogen also leads to methane production. The rate of solid methane formation is described by Equations (5) and (6). Assuming that reaction (4) controls the hydrogasification mechanism and reaction (3) is in an equilibrium state, Equation (5) may be presented as follows:

$$k_{3f} [C_f] p_{\text{H}_2} - k_{3b} [\text{C}(\text{H}_2)] = 0 \quad (22)$$

when  $\text{C}(\text{H}_2)$  in Equation (6) is expressed by  $[C_f]$  from Equation (22), the hydrogasification rate is described as:

$$\dot{R}_4 = n_C [C_f] \left[ k_{4f} \frac{k_{3f}}{k_{3b}} p_{\text{H}_2}^2 - k_{4b} p_{\text{CH}_4} \right], \text{ kmol s}^{-1} \quad (23)$$

Equation (23) describes the rate of C gasification ( $\text{mol}_C \text{ s}^{-1}$ ) as equal to the rate of methane production ( $\text{mol}_{\text{CH}_4} \text{ s}^{-1}$ ). For a constant number of free active centers  $[C_f]$  per unit of C mass in the char particle, the final kinetic equation may be defined as follows:

$$\dot{R}_4 = n_C [A(T) p_{\text{H}_2}^2 - B(T) p_{\text{CH}_4}], \text{ kmol s}^{-1} \quad (24)$$

where  $A(T) = [C_f] k_{4f} (k_{3f} k_{3b}^{-1})$  and  $B(T) = [C_f] k_{4b}$  are experimentally determined kinetic constants. However, it is highly possible that the total number of active centers  $[C_t] = [C_f] + [\text{C}(\text{H}_2)]$

per unit of C mass is constant. Using the total number of active centers in Equation (22) and substituting  $[C_t]$  for  $[C_f]$  and  $[C(H_2)]$ , the rate of hydrogasification can be presented as:

$$\dot{R}_4 = n_C \frac{k_{4f} \frac{k_{3f}}{k_{3b}} p_{H_2}^2 - k_{4b} p_{CH_4}}{1 + \frac{k_{3f}}{k_{3b}} p_{H_2}}, \text{ kmol s}^{-1} \quad (25)$$

and its final form:

$$\dot{R}_4 = n_C \frac{C(T) p_{H_2}^2 - D(T) p_{CH_4}}{1 + E(T) p_{H_2}}, \text{ kmol s}^{-1} \quad (26)$$

The coefficients of hydrogasification rate  $C(T) = [C_t]k_{4f}(k_{3f} k_{3b}^{-1})^{-1}$ ,  $D(T) = [C_t]k_{4b}$ , and  $E(T) = k_{3f} k_{3b}^{-1}$  were determined based on experiments conducted at various hydrogen pressures and process temperatures. The number of generated methane moles was determined based on the equation:

$$n_{CH_4} = \dot{n}_g \int_0^t z_{CH_4}(t) dt, \text{ kmol} \quad (27)$$

while the number of carbon moles in the sample at time  $t$  is determined by the Equation (13).

For the above model, an algorithm for computer calculation was developed to enable the determination of the kinetic constants. Based on the results of a series of experiments, the kinetic constants of gaseous hydrogasification product formation were determined using the values at the points of maximum process reactivity. The kinetic constants for Janina coal char from the paper by Tomeczek and Gil [31] (see Table 6) were used to determine correlations for the Equation (26) presented in Figure 11.

**Table 6.** Hydrogasification reactivity kinetic constants [31].

Constant	$A(T)$	$B(T)$	$C(T)$	$D(T)$	$E(T)$
$E, \text{ kJ mol}^{-1}$	40	129	122	211	85
$(\text{Pa}^2\text{s})^{-1}$	$3.0 \times 10^{-16}$		$2.1 \times 10^{-8}$		
$k_0$	$(\text{Pa s})^{-1}$		$1.4 \times 10^{-5}$	$9.5 \times 10^{-2}$	
	$\text{Pa}^{-1}$				$1.6 \times 10^{-1}$

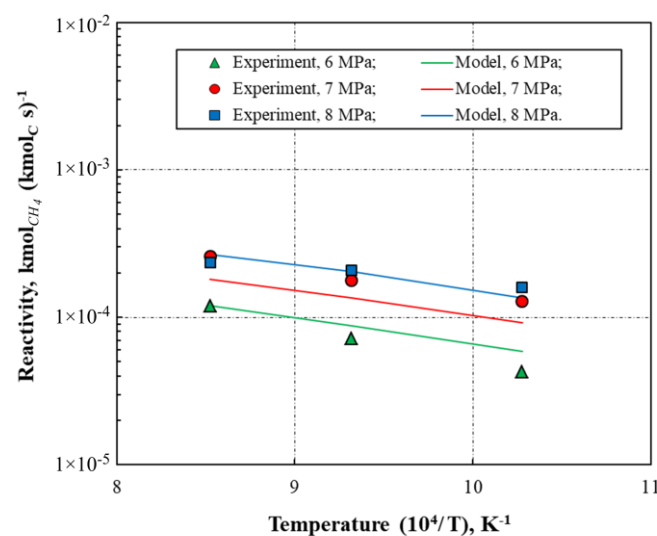


**Figure 11.** Hydrogasification reactivity: the Janina char,  $2 \text{ dm}_n^3 \text{ min}^{-1}$ , 0.6–1.0 mm.

A contrast of the kinetic Equation (26) is shown in Figure 12 formulated for the Janina char ( $p_{\text{H}_2} = 6 \text{ MPa}$ ,  $p_{\text{CH}_4} = 0 \text{ MPa}$ ) with data from two sources in the literature: Mühlen [20], Fürst Leopold char,  $p_{\text{H}_2} = 6 \text{ MPa}$ ,  $p_{\text{CH}_4} = 0 \text{ MPa}$ , and Misirlioglu et al. [4], Elbistan char,  $p_{\text{H}_2} = 2.5 \text{ MPa}$ ,  $p_{\text{CH}_4} = 0 \text{ MPa}$ . The reactivity values for the investigated Janina char are similar to those computed by Mühlen [20] for the ‘Fürst Leopold’ char, also for conversion  $U=0$ , and they surpass the values reported for the “Elbistan” char [14] by more than one order of magnitude. In comparison to the other shown chars, the ‘Fürst Leopold’ char exhibits a significantly higher activation energy for the overall process  $\text{C} + 2\text{H}_2 \rightleftharpoons \text{CH}_4$ .

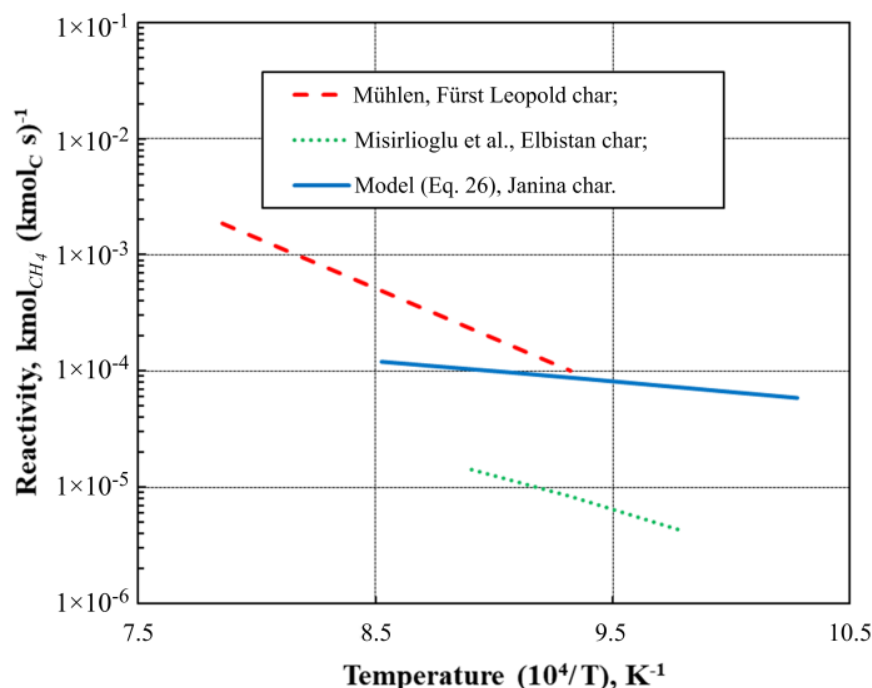


Figure 12. A comparison of the char reactivity values. Adapted from [4,10].

## 5. Discussion of the Results

Figure 5 shows the velocity vectors of the hydrogen stream flowing through the swirl system (operating temperature  $T = 973 \text{ K}$  and operating pressure  $p = 6 \text{ MPa}$ ). The obtained speeds ranged from  $0.1$  to  $0.3 \text{ m s}^{-1}$ . Values in the upper range occur most often between the swirl insert and the reactor wall.

The obtained temperature field indicates that hydrogen is heated to the desired temperature in the short initial section of the reactor, but only in the outer layer. This is due to the higher velocities of the gas flowing at the wall (Figure 7), while the core of the flowing gas block has a slightly lower temperature of approx.  $1150 \text{ K}$ .

Figure 7 shows the velocity vectors of the hydrogen stream for higher values of pressure and temperature (operating temperature  $T = 1273 \text{ K}$  and operating pressure  $p = 10 \text{ MPa}$ ) than in Figure 5. Due to the higher density of the flowing gas under the pressure of  $10 \text{ MPa}$  with the same mass streams, the obtained velocities were lower and ranged from  $0.03$  to  $0.2 \text{ m s}^{-1}$ .

The results of temperature influence on the carbon conversion rate were contrasted with those reported by Ding et al. [35] for the ‘Inner Mongolia Semicoke’ under the same conditions and at  $5 \text{ MPa}$  (Figure 8). The highest conversion rate for the Janina char was similar to that reported by Ding et al., while it was lower by  $18\%$  at  $1173 \text{ K}$ .

Figure 10 shows the computed char reactivity for two temperature values,  $1073$  and  $1173 \text{ K}$ , and the hydrogasification pressure of  $7$  and  $8 \text{ MPa}$  as a function of carbon conversion. When the carbon conversion exceeds  $60\%$  or  $80\%$ , respectively, for  $1073 \text{ K}$  and especially for  $1173 \text{ K}$ , the reactivity rapidly decreases. This implies that a temperature of roughly  $1200 \text{ K}$

needs to be maintained in order to achieve a significant amount of carbon conversion during char hydrogasification; however, the upper temperature range for the reactor used did not allow for such experiments.

For the presented hydrogasification model, an algorithm for computer calculation was developed to enable the determination of the kinetic constants. The presented hydrogasification algorithm uses mechanisms of structural change such as particle porosity, internal specific surface area, total active centers, and degree of carbon conversion. Based on the results of a series of experiments, the kinetic constants of gaseous hydrogasification product formation were determined using the values at the points of maximum process reactivity. The kinetic constants for Janina coal char from the paper by Tomeczek and Gil [31] (see Table 6) were used to determine correlations for the Equation (26) presented in Figure 11. The developed kinetic equations based on these dependencies can be used to model the process on a technical scale.

A contrast of the kinetic Equation (26) is shown in Figure 12, formulated for the Janina char, with data from two sources in the literature: Mühlen [20], Fürst Leopold char, and Misirlioglu et al. [4], Elbistan char. The reactivity values for the investigated Janina char are similar to those computed by Mühlen [20] for the 'Fürst Leopold' char, also for conversion equal to 0, and they surpass the values reported for the "Elbistan" char [14] by more than one order of magnitude. In comparison to the other shown chars, the 'Fürst Leopold' char exhibits a significantly higher activation energy for the overall process of hydrogasification.

## 6. Conclusions

Since hydrogen is heated only by convection ( $H_2$  is transparent to radiation), it is important to properly design the heater in the gas supply line to the hydrogasification process and to control its temperature.

The char becomes less reactive with prolonged contact with hydrogen. Probably, hydrogasification requires temperatures higher than 1200 K to achieve a high degree of coal conversion; however, the upper temperature range for the reactor used did not allow for such experiments.

At 973 K, the hydrogasification process is more than two times less than at 1173 K; thus, hydrolysis produces more methane at higher temperatures than hydrogasification does at lower temperatures; the situation is inverted during char hydrogasification, which produces a lot more methane.

The influence of temperature on the carbon conversion rate was contrasted with those reported by Ding et al. [35] for the 'Inner Mongolia Semicoke' under the same conditions and at 5 MPa. The highest conversion rate for the Janina char was similar to that reported by Ding et al., while it was lower by 18% at 1173 K.

Equations for both the first- and second-order reactions toward hydrogen may accurately represent the maximal hydrogasification reactivity of chars. This is likely due to the use of a limited pressure range in the experiments, whereas, due to the partial pressure of hydrogen, it is more likely to fit the first-order equation.

The presented hydrogasification algorithm uses mechanisms of structural change such as particle porosity, internal specific surface area, total active centers, and degree of carbon conversion. The developed kinetic equations based on these dependencies can be used to model the process on a technical scale.

To further improve the efficiency of the hydrogasification process, the next step should be tests involving catalysts.

**Author Contributions:** Conceptualization, S.G., P.M. and W.B.; methodology, S.G.; software, P.M., N.P. and W.B.; validation, S.G., J.K. and M.R.; formal analysis, S.G.; investigation, S.G., P.M. and W.B.; resources, J.K., N.P. and M.R.; data curation, S.G. and P.M.; writing—original draft preparation, S.G., W.B. and P.M.; writing—review and editing, S.G., W.B. and J.K.; visualization, W.B. and J.K.; supervision, S.G.; project administration, S.G.; funding acquisition, S.G. and W.B. All authors have read and agreed to the published version of the manuscript.

**Funding:** This research received no external funding.

**Data Availability Statement:** The study did not report any data.

**Conflicts of Interest:** The authors declare no conflict of interest.

## References

1. European Parliament. Fact Sheets on the European Union. Energy Policy: General Principles. 2023. Available online: <https://www.europarl.europa.eu/factsheets/en/sheet/68/energeticka-politika-vseobecne-zasady> (accessed on 20 March 2023).
2. Tosti, S.; Spazzafumo, G.; Capobianco, D.; Buceti, G.; Pozio, A.; Bartucca, S. EU scenarios of renewable coal hydro-gasification for SNG production. *Sustain. Energy Technol. Assess.* **2016**, *16*, 43–52. [[CrossRef](#)]
3. Škvareková, E.; Wittenberger, G.; Šofranko, M. Tar related issues in underground coal gasification. *Acta Montan. Slovaca* **2016**, *21*, 298–305.
4. Kapusta, K.; Wiatowski, M.; Thomas, H.R.; Zagorscak, R.; Sadasivam, S.; Masum, S.; Kempka, T.; Otto, C.; Basa, W.; Szyja, M.; et al. Experimental simulations of methane-oriented underground coal gasification using hydrogen- The effect of coal rank and gasification pressure on the hydrogasification process. *Int. J. Hydrog.* **2023**, *48*, 921–932. [[CrossRef](#)]
5. Wiatowski, M. An Experimental Study on the Quantitative and Qualitative Characteristics of Tar Formed during Ex Situ Coal Gasification. *Energies* **2023**, *16*, 2777. [[CrossRef](#)]
6. Pástor, M.; Lukáč, L.; Jablonský, G.; Furka, F. Design of equipment and methodology for secondary tar removal after gasification in low heat output generators. *Adv. Therm. Process. Energy Transform.* **2019**, *2*, 57–60. [[CrossRef](#)]
7. Mlonka-Medrala, A.; Evangelopoulos, P.; Sieradzka, M.; Zajemska, M.; Magdziarz, A. Pyrolysis of agricultural waste biomass towards production of gas fuel and high-quality char: Experimental and numerical investigations. *Fuel* **2021**, *296*, 120611. [[CrossRef](#)]
8. Slowak, A.M. Innovative Method of Forecasting the Generator Gas Composition after the Process of Pyrolysis and Gasification. *Rocz. Ochr. Sr.* **2022**, *24*, 97–109. [[CrossRef](#)]
9. Saraceno, E.; Ruocco, C.; Palma, V. A Review of Coal and Biomass Hydrogasification: Process Layouts, Hydrogasifiers, and Catalysts. *Catalysts* **2023**, *13*, 417. [[CrossRef](#)]
10. Liu, X.; Xiong, B.; Huang, X.; Ding, H.; Zheng, Y.; Liu, Z.; Zheng, C. Effect of catalysts on char structural evolution during hydrogasification under high pressure. *Fuel* **2017**, *188*, 474–482. [[CrossRef](#)]
11. Lee, S.H.; Lee, J.G.; Kim, J.H.; Choi, Y.C. Hydrogasification characteristics of bituminous coals in a entrained flow hydrogasifier. *Fuel* **2006**, *85*, 803–806. [[CrossRef](#)]
12. Xu, W.C.; Matsuoka, K.; Akiho, H.; Kumagai, M.; Tomita, A. High pressure hydro-pyrolysis of coals by using a continuous free-fall reactor. *Fuel* **2003**, *82*, 677–685. [[CrossRef](#)]
13. Karcz, A.; Porada, S. The influence of coal rank on formation of gaseous hydrocarbons in hydrogasification of coal. *Fuel* **1996**, *75*, 641–645. [[CrossRef](#)]
14. Misirlioglu, Z.; Canel, M.; Sinağ, A. Hydrogasification of chars under high pressures. *Energy Convers. Manag.* **2007**, *48*, 52–58. [[CrossRef](#)]
15. Gonzales, J.F.; Ramiro, A.; Sabio, E.; Encinar, J.M.; Gonzales, C.M. Hydrogasification of Almond Shell Chars, Influence of Operating Variables and Kinetic Study. *Ind. Eng. Chem. Res.* **2002**, *41*, 3557–3565. [[CrossRef](#)]
16. Suuberg, E.M.; Peters, W.A.; Howard, J.B. Product compositions in rapid hydro-pyrolysis of coal. *Fuel* **1980**, *59*, 405–412. [[CrossRef](#)]
17. Blackwood, J.D.; Mc Carthy, D.J. The mechanism of hydrogenation of coal to methane. *Aust. J. Chem.* **1966**, *19*, 797–813. [[CrossRef](#)]
18. Blackwood, J.D. The kinetics of the system carbon hydrogen methane. *Aust. J. Chem.* **1962**, *15*, 397–408. [[CrossRef](#)]
19. Laurendeau, N.M. Heterogeneous kinetics of coal char gasification and combustion. *Prog. Energy Combust. Sci.* **1978**, *4*, 221–270. [[CrossRef](#)]
20. Mühlen, H.J. Zum Einfluß der Produktgase auf die Kinetic der Wasserdampfvergasung in Abhängigkeit von Druck und Temperatur. Ph.D. Thesis, Bergbau-Forschung GmbH, Essen, Germany, 1983.
21. Tomita, A.; Mahajan, O.P.; Walker, P.L., Jr. Reactivity of heat-treated coals in hydrogen. *Fuel* **1977**, *56*, 137–144. [[CrossRef](#)]
22. Moseley, F.; Paterson, D. The rapid high-temperature hydrogenation of coal chars, Part 1: Hydrogen pressures up to 100 atmospheres. *J. Inst. Fuel* **1965**, *1*, 13–23.
23. Mühlen, H.J.; Van Heek, K.H.; Jüntgen, H. Influence of pretreatment temperature and pressure on the char reactivity during hydrogasification. *Fuel* **1986**, *65*, 591–593. [[CrossRef](#)]
24. Johnson, J.L. *Kinetics of Coal Gasification*; John Wiley and Sons: Hoboken, NJ, USA, 1979.
25. Tomajian, M.E.; Lussier, M.G.; Miller, D.J. Effect of oxidation and other treatments on hydrogasification rate of coal char. *Fuel* **1992**, *71*, 1055–1061. [[CrossRef](#)]
26. Blackwood, J.D. The reaction of carbon with hydrogen at high pressure. *Aust. J. Chem.* **1959**, *12*, 14–28. [[CrossRef](#)]
27. Porada, S. A comparison of basket willow and coal hydrogasification and pyrolysis. *Fuel Process. Technol.* **2009**, *90*, 717–721. [[CrossRef](#)]
28. Tosti, S.; Sousa, M.A.; Buceti, G.; Madeira, L.M.; Pozio, A. Process analysis of refuse derived fuel hydrogasification for producing SNG. *Int. J. Hydrog. Energy* **2019**, *44*, 21470–21480. [[CrossRef](#)]

29. Yan, S.; Qu, X.; Xia, Z.; Chen, C.; Bi, J. Effect of experimental variables on coal catalytic hydrogasification in a pressurized fluidized bed. *Fuel* **2022**, *307*, 121761. [[CrossRef](#)]
30. Xia, Z.; Yan, S.; Chen, C.; Qu, X.; Bi, J. Three-dimensional simulation of coal catalytic hydrogasification in a pressurized bubbling fluidized bed. *Energy Convers. Manag.* **2021**, *250*, 114874. [[CrossRef](#)]
31. Tomeczek, J.; Gil, S. The kinetics of coal chars hydrogasification. *Fuel Process. Technol.* **2010**, *91*, 1564–1568. [[CrossRef](#)]
32. Gil, S.; Mocek, P.; Bialik, W. Changes in total active centers on particle surfaces during coal pyrolysis, gasification and combustion. *Chem. Process Eng.* **2011**, *32*, 155–169. [[CrossRef](#)]
33. Stanmore, B.R. Modeling of combustion behavior of petroleum coke. *Combust. Flame* **1991**, *83*, 221–227. [[CrossRef](#)]
34. Johnson, J.L. Relationship between the gasification reactivities of coal char and the physical and chemical properties of coal and coal char. *Am. Chem. Soc. Div. Fuel Chem.* **1975**, *20*, 85–102.
35. Ding, X.; Zhang, Y.; Zhang, T.; Tang, J.; Xu, Y.; Zhang, J. Effect of operational variables on the hydrogasification of inner Mongolian lignite semicoke. *Energy Fuels* **2013**, *27*, 4589–4597. [[CrossRef](#)]

**Disclaimer/Publisher’s Note:** The statements, opinions and data contained in all publications are solely those of the individual author(s) and contributor(s) and not of MDPI and/or the editor(s). MDPI and/or the editor(s) disclaim responsibility for any injury to people or property resulting from any ideas, methods, instructions or products referred to in the content.